

Coulomb explosion of nanodroplets drives the conversion of laser energy to nuclear energy

Isidore Last¹, Shlomo Ron¹, Andreas Heidenreich^{2,3}, and Joshua Jortner¹

¹School of Chemistry, Tel Aviv University, Ramat Aviv, 69978 Tel Aviv, Israel

²Kimika Fakultatea, Euskal Herriko Unibertsitatea (UPV/EHU) and Donostia International Physics Center (DIPC), P.K. 1072, 20080 Euskadi, Spain

³IKERBASQUE, Basque Foundation for Science, 48011 Bilbao, Spain

(Received 15 April 2013; revised 20 May 2013; accepted 6 June 2013)

Abstract

Theoretical–computational studies of table-top laser-driven nuclear fusion of high-energy (up to 15 MeV) deuterons with ⁷Li, ⁶Li, and D nuclei demonstrate the attainment of high fusion yields within a source–target reaction design. This constitutes a source of Coulomb-exploding deuterium nanodroplets driven by an ultraintense femtosecond near-infrared laser and a solid hollow cylindrical target containing the second element. The source–target reaction design attains the highest table-top fusion efficiencies (up to 4×10^9 J⁻¹ per laser pulse) obtained to date. The highest conversion efficiency of laser energy to nuclear energy (10^{-2} – 10^{-3}) for table-top DD fusion attained in the source–target design is comparable to that for DT fusion currently accomplished for ‘big science’ inertial fusion setups.

Keywords: Coulomb explosion; nanodroplets and clusters; source-target design; table top nuclear fusion; ultraintense lasers

1. Introduction

Table-top nuclear fusion in the chemical physics laboratory^[1,2] was realized by nuclear fusion driven by Coulomb explosion (NFDCE) of assemblies of nanostructures, i.e., clusters (with initial radii $R_0 = 1$ – 10 nm)^[3–15], and nanodroplets (with $R_0 = 10$ – 500 nm)^[15–20], which are driven by ultraintense femtosecond near-infrared lasers^[7,8,17]. The ultraintense laser pulses for generating Coulomb explosion (CE) of such nanostructures are characterized by ultrahigh intensities of up to 10^{21} W · cm⁻², which can be produced from the currently available Terawatt and Pentawatt lasers^[21]. The interaction of ultraintense femtosecond near-infrared lasers with nanometer-sized matter^[2–20] results in inner and outer ionization of the nanostructures^[22–24] followed by CE, which produces high-energy (10 keV–15 MeV) ions in the energy domain of nuclear physics. Previous studies of NFDCE of clusters^[2–15] and of nanodroplets^[17–20,24] involved nuclear reactions inside or outside the macroscopic plasma filament, which is produced by an assembly of Coulomb-exploding nanostructures within the focal volume of the laser.

NFDCE constitutes the table-top conversion of laser energy to nuclear energy. We advance theoretical–computational methods to establish the conditions for the attainment

of high efficiencies for table-top conversion of laser energy to nuclear energy mediated by CE dynamics of molecular nanodroplets. A source–target design^[25,26] for fusion of D with ⁷Li, ⁶Li, and D atoms attains the highest table-top fusion efficiencies ($\sim 10^9$ J⁻¹ per laser pulse) obtained to date. The data for high-efficiency table-top laser energy → nuclear energy conversion are comparable to those obtained to date for ‘big science’ inertial fusion setups^[27–30].

2. The source–target design for table-top fusion

Our exploration of the maximization of table-top fusion yields^[26] established that an increase of the table-top fusion efficiencies by 3–5 orders of magnitude for NFDCE of nanodroplets, relative to those attained inside or outside a plasma filament^[2,6,7,11,19,23], can be attained by transcending the macroscopic plasma filament as a reaction medium for table-top fusion and by considering a source–target design, which was advanced in our previous work^[25,26], with the following operational conditions.

- (1) The source–target design is based on the selection of an appropriate source (where high-energy deuterons or protons are produced by CE) and a target (where the fusion reaction occurs). For fusion between two distinct nuclei, high-energy deuterons (or protons) are produced with the source by CE of homonuclear deuterium or

Correspondence to: Joshua Jortner, School of Chemistry, Tel Aviv University, Ramat Aviv, 69978 Tel Aviv, Israel.
Email: jortner@post.tau.ac.il

hydrogen nanodroplets^[25,26]. The ions react with a solid target of the second reagent.

- (2) Regarding the properties of the source within the source–target design, a key element for efficient fusion rests on the production of high-energy (up to 15 MeV) deuterons or protons^[24].
- (3) The beneficial properties of the cylindrical hollow solid target within the source–target design originate from the efficient collection of high-energy deuterons and protons from the source, together with the moderately low stopping power and large penetration depth of deuterons within the solid^[25,26].

3. Table-top fusion yields

High table-top fusion yields were calculated for reactions of deuterons with several light nuclei, i.e., ⁷Li, ⁶Li, and D, within the source–target reaction design^[25,26]. The source consists of deuterons produced by CE of deuterium nanodroplets, $R_0 = 70\text{--}300$ nm, impinging on a hollow solid cylinder target containing the ⁷Li, ⁶Li, and D atoms. The fusion reactions with the highest cross sections in the relevant energy domains^[31–33] were considered. The cylindrical solid target involves ⁷Li or ⁶Li (pure metal or LiF ionic solid) for reactions of D with Li isotopes, and low-temperature ($T < 20$ K) deuterium film or deuterated (CD₂) polymer polyethylene^[2,13,26] at room temperature for the D+D reaction.

The fusion reaction yield Y per laser pulse is

$$Y = N\langle y \rangle, \quad (1)$$

where N is the number of deuterons produced from the source and $\langle y \rangle$ is the average reaction probability:

$$\langle y \rangle = \int_0^{E_{\max}} P(E)y(E)dE. \quad (2)$$

Here $P(E)$ is the energy distribution function of the ions with a maximal energy E_{\max} , obtained from scaled electron and ion dynamics (SEID) simulations described in our previous work^[24,34,35], and $y(E)$ is the reaction probability per ion with an initial energy E penetrating into the solid target, given by

$$y(E) = \int_0^E \frac{\sigma(E')}{S(E')} dE', \quad (3)$$

where $\sigma(E)$ is the reaction cross section^[31–33] and $S(E)$ is the stopping power normalized to the atomic density of the target^[36]. The energy dependence of $y(E)$ (inset to Figure 1) over the relevant energy domain up to 15 MeV (which corresponds to the CE energies) is determined by the cumulative contributions of $\sigma(E)$ and $S(E)$. $y(E)$ exhibits a nearly power-law dependence on E (inset to Figure 1), in the form

$$y(E) = bE^\xi, \quad (4)$$

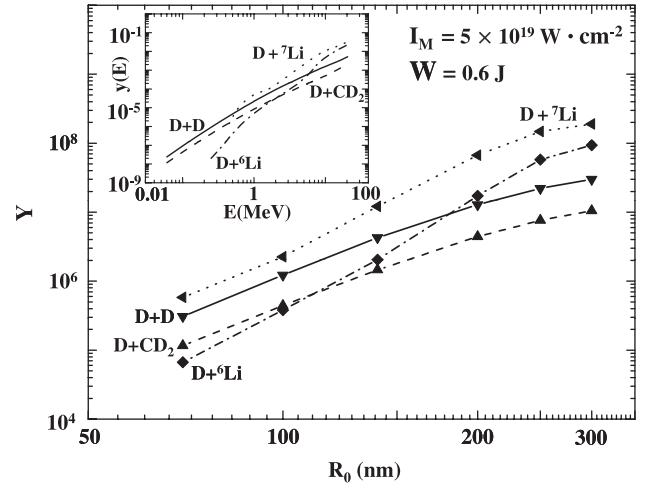


Figure 1. Nanodroplet size dependence of the table-top fusion yields Y , Equation (1), within the source–target design for the fusion of deuterons with a solid hollow cylinder of ⁷Li, ⁶Li, solid deuterium, and deuterated polyethylene (CD₂), as marked on the curves. The laser parameters are $I_M = 5 \times 10^{19} \text{ W} \cdot \text{cm}^{-2}$, $\tau = 30$ fs, and $W = 0.6$ J. The inset shows the energy dependence of the fusion reaction probability $y(E)$.

where b is a constant and ξ is a scaling parameter. The data of the inset to Figure 1 result in $\xi = 1.8 \pm 0.3$ for D+D, $\xi = 2.2 \pm 0.7$ for D+⁷Li and $\xi = 2.9 \pm 0.7$ for D+⁶Li. For the conditions of complete vertical outer ionization (CVI) of the nanodroplet^[2,22–24], the CE energetics is determined by electrostatic models^[2,22,23]. Under CVI conditions the kinetic energy distribution of the deuterons is^[2,22,23] $P(E) = (3/2E_{\max})(E/E_{\max})^{1/2}$ for $0 < E \leq E_{\max}$, with the maximal kinetic energy being^[2,29,30] $E_{\max} = aR_0^2$, where $a = (4\pi/3)\bar{B}\rho_{\text{mol}}q^2$, with $\bar{B} = 1.44 \times 10^{-3}$ keV nm, ρ_{mol} is the initial density of the nanostructure, and $q = 1$ is the ion charge. The validity of the CVI relations for the energetics of CE is borne out of SEID simulations^[24,26,34,35], which include intra-nanodroplet intensity attenuation^[24] and relativistic effects^[37,38]. Equations (1), (2) and (4), together with the CVI relations for E_{\max} and $P(E)$, result in

$$Y = [N/(\zeta + 3/2)]baR_0^\zeta \quad (5)$$

with

$$\zeta = 2\xi. \quad (6)$$

Equation (5) predicts a power law for the nanodroplet size dependence of the fusion yields, with the scaling parameter ζ being given by Equation (6).

The fusion yields, Equation (1), were calculated from

- (i) the $y(E)$ data of Equation (3) (presented in the inset to Figure 1), and the $P(E)$ functions obtained from SEID simulations, which result in $\langle y \rangle$, Equation (2);
- (ii) the number N of the deuterons produced from the Coulomb-exploding source.

N is governed by laser energy deposition inside the plasma filament within the laser focal volume^[25,26]. The

fraction β of the laser energy acquisition by the assembly of nanodroplets is^[25,26] $\beta = NE_{\text{abs}}/W$ with $0 \leq \beta \leq 1$, where W is the laser pulse energy and E_{abs} is the laser energy absorbed per atom within a nanodroplet, which was obtained from SEID simulations for exploding deuterium nanodroplets, while the laser parameters are the peak intensity $I_M = 5 \times 10^{19} \text{ W} \cdot \text{cm}^{-2}$, pulse duration $\tau = 3 \times 10^{-14} \text{ s}$, pulse energy $W = 0.6 \text{ J}^{[17]}$, and laser wavelength $\lambda = 8 \times 10^{-5} \text{ cm}$. Following our previous work^[26], the number of deuterons within the macroscopic plasma filament is

$$N = 3.54(\rho/\lambda)(W/I_M\tau)^2; \quad \beta < 1 \quad (7a)$$

for the weak assembly intensity attenuation, and

$$N = W/E_{\text{abs}}; \quad \beta = 1 \quad (7b)$$

for the strong assembly intensity attenuation. Here, the macroscopic plasma filament is characterized by the deuteron density, where $\rho = 3 \times 10^{18} \text{ cm}^{-3}$ ^[17].

The nanodroplet size dependence of the fusion yields was calculated for the laser and nanoplasma parameters given above. For these input data, the weak assembly attenuation limit $\beta < 1$ is strictly applicable over the entire size domain^[26]. Furthermore, for the highest laser intensity $I_M = 5 \times 10^{19}$, the CVI relation is nearly applicable up to $R_0 = 300 \text{ nm}$, whereupon Equation (5) is applicable for the analysis of the yield data. The nanodroplet size dependence of Y portrayed in Figure 1 exhibits a nearly linear dependence of $\log Y$ versus $\log R_0$, resulting in a power-law size dependence of Y on R_0 , of the form $Y \propto R_0^\zeta$. The scaling parameters ζ obtained for Figure 1 are $\zeta = 3.3 \pm 0.5$ for D+D, $\zeta = 4.5 \pm 0.7$ for D+⁷Li, and $\zeta = 5.4 \pm 0.6$ for D+⁶Li. These scaling parameters ζ , obtained for the nanodroplet size dependence of Y , obey the relation $\zeta = 2\xi$, where ξ , Equation (4), are the scaling parameters for the energy dependence reaction probability, Equation (3), which are presented above. This result is in accord with the relation predicted by Equation (6).

4. Fusion efficiencies and their dependence on the laser pulse energy

The fusion efficiency^[15,26,39] is

$$\Phi = Y/W. \quad (8)$$

The fusion yields and efficiencies were maximized for the nanodroplet size and the laser parameters. Our results for Y (Figure 1) and Φ were obtained at a fixed laser pulse energy of $W_0 = 0.6 \text{ J}^{[17]}$ and at a high laser intensity of $I_M = 5 \times 10^{19} \text{ W} \cdot \text{cm}^{-2}$. We shall now advance a scaling method for the dependence of Y and Φ on the laser pulse energy W for the domains of weak assembly intensity attenuation ($\beta < 1$) and strong assembly intensity attenuation ($\beta = 1$). Increasing W beyond W_0 is expected to increase Y and Φ for $\beta < 1$ in the range $W_0 < W \leq W_M$, while for $\beta = 1$ a distinct dependence of the parameters on W is

realized in the range $W > W_M$. W_M marks the laser power for the ‘transition’ from $\beta < 1$ to $\beta = 1$, which is given by^[26]

$$W_M = (I_M\tau)^2 / 3.54(\rho/\lambda)E_{\text{abs}}. \quad (9)$$

A typical value of $W_M = 8 \text{ J}$ for the largest nanodroplet size and highest intensity, i.e., $R_0 = 300 \text{ nm}$ and $I_M = 5 \times 10^{19} \text{ W} \cdot \text{cm}^{-2}$, was estimated from Equation (9). The W scaling of $Y(W)$ and of $\Phi(W)$ is obtained in the form^[26]

$$Y(W)/Y(W_M) = (W/W_M)^2; \quad W_0 < W \leq W_M, \quad (10a)$$

$$\Phi(W)/\Phi(W_M) = (W/W_M); \quad W_0 < W \leq W_M, \quad (11a)$$

and

$$Y(W)/Y(W_M) = (W/W_M); \quad W > W_M, \quad (10b)$$

$$\Phi(W)/\Phi(W_M) = 1; \quad W > W_M. \quad (11b)$$

Accordingly, the calculation of the maximal value of Φ will be achieved by SEID simulations for the optimization of Y and Φ at a fixed laser pulse energy ($W_0 < W_M$), followed by the W scaling of these attributes from W_0 to W_M . The maximal value of Φ is $\Phi(W_M)$. Our results for $Y(W_M)$ and $\Phi(W_M)$ were obtained from the scaling of the SEID simulation results at $W_0 = 0.6 \text{ J}$ (Figure 2). The optimal fusion yields per laser pulse (for the nanodroplet size $R_0 = 300 \text{ nm}$, and laser parameters $I_M = 5 \times 10^{19} \text{ W} \cdot \text{cm}^{-1}$, $\tau = 30 \text{ fs}$, and $W_M = 8 \text{ J}$) are $Y(W_M) = 3.4 \times 10^{10}$, 1.7×10^{10} , and 5.3×10^9 for the fusion of D with ⁷Li, ⁶Li, and D, respectively. Our analysis then results in the attainment of the maximal high table-top fusion efficiencies, i.e., $\Phi(W_M) = 4 \times 10^9 \text{ J}^{-1}$, $2 \times 10^9 \text{ J}^{-1}$, and $7 \times 10^8 \text{ J}^{-1}$ for the fusion of D with ⁷Li, ⁶Li, and D, respectively.

The maximal value of the laser energy to nuclear energy conversion efficiency for table-top fusion is

$$\Psi(W_M) = \Phi(W_M)Q, \quad (12)$$

where Q is the energy release in the nuclear reaction and $\Phi(W_M) = Y(W_M)/W_M$. The estimates for $\Psi(W_M)$ for the fusion of D with ⁷Li, ⁶Li, and D are 1.0×10^{-2} , 1.1×10^{-3} , and 3.9×10^{-4} , respectively.

5. Discussion

Of considerable interest is the attainment of high efficiencies for the conversion of laser energy to nuclear energy. Two major conclusions regarding records for table-top fusion emerge from our analysis.

- (1) Records for table-top conversion of laser energy to nuclear energy. Our theoretical–computational studies demonstrate the attainment of high fusion efficiencies in the range $\Phi(W_M) \simeq 10^9 \text{ J}^{-1}$ for the fusion reaction of D with ⁷Li, ⁶Li, and D. These data constitute the highest table-top fusion yields and efficiencies obtained to date. The source–target design, constituting of an exploding nanodroplets source driven by a superintense laser and a

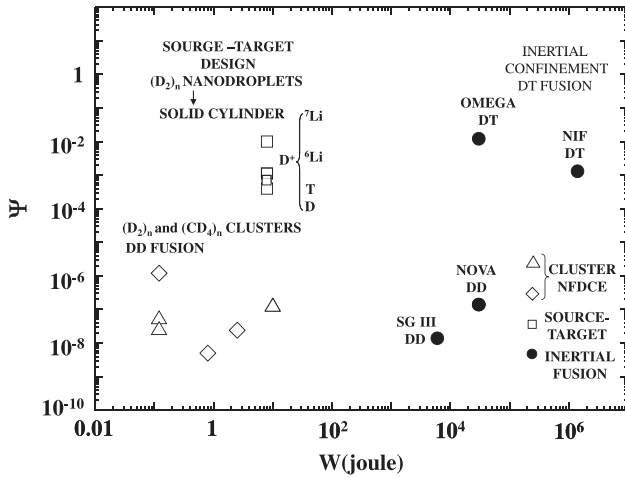


Figure 2. A record of the currently available data for the dependence of the efficiency Ψ of conversion of laser energy to nuclear energy on the laser pulse energy W for table-top fusion driven by CE of nanodroplets and in a source–target design. A comparison is presented between experimental data for DD fusion driven by CE of $(D_2)_n$ and $(CD_4)_n$ clusters inside and outside a macroscopic plasma filament^[5–8], theoretical–computational data for fusion of deuterium with light atoms ${}^7\text{Li}$, ${}^6\text{Li}$, T, and D within the source–target design (present work and reference 26), and of experimental data for DT and DD inertial fusion in ‘big science’ inertial fusion setups^[28–30].

solid hollow cylinder target, provides the most efficient device for the table-top conversion of laser energy to nuclear energy.

- (2) Table-top laser \rightarrow nuclear conversion efficiency is comparable to that in giant fusion machines attained to date. The table-top laser energy \rightarrow nuclear energy conversion efficiency within the source–target design is comparable to that obtained to date in the ‘big science’ setups for inertial fusion^[27–30]. This is evident from the currently available data (Figure 2), where the table-top ‘big science’ fusion Ψ data fall into two domains characterized by different laser pulse powers: (i) the lower pulse power range ($W = 0.1\text{--}10$ J) for table-top cluster NFDCE and for the source–target design; and (ii) the high pulse power range ($W = 6 \times 10^3\text{--}3 \times 10^6$ J) for ‘big science’ inertial fusion. From the outline portrayed in Figure 2, we infer that high values of $\Psi(W_M)$, in the range $10^{-2}\text{--}10^{-3}$, can be attained for the fusion of D with ${}^7\text{Li}$, ${}^6\text{Li}$, and D (Section 4), and with T^[26] within the table-top source–target design with a source of Coulomb-exploding large deuterium nanodroplets ($R_0 = 300$ nm) driven by a superintense laser ($I_M = 5 \times 10^{19}$ W \cdot cm $^{-2}$ and $W_M = 8$ J). These high $\Psi(W_M)$ results for the table-top source–target design fall within ~ 1 order of magnitude in comparison with those obtained for DT fusion in ‘big science’ setups, i.e., in the OMEGA laser system ($W = 30$ kJ, $Y = 10^{14}$, $\Phi = 3 \times 10^9$ J $^{-1}$, and $\Psi = 1.2 \times 10^{-2}$ ^[28]) and in the National Ignition

Facility (NIF) system ($W = 1.43$ MJ, $Y = 6 \times 10^{14}$, $\Phi = 4.1 \times 10^8$, and $\Psi = 1.3 \times 10^{-3}$ ^[29]).

Acknowledgements

This research was supported by the Binational German–Israeli James Franck Program on laser–matter interaction at Tel-Aviv University and by the Spanish Ministry of Science and Education (MICINN) and by the SAIOTEK Program of the Basque government at the University of the Basque Country.

References

1. J. Jortner, and I. Last, *ChemPhysChem* **3**, 845 (2002).
2. A. Heidenreich, I. Last, and J. Jortner, *Proc. Natl. Acad. Sci. USA* **103**, 10589 (2006).
3. J. Zweiback, R. A. Smith, T. E. Cowan, G. Hays, K. B. Wharton, V. P. Yanovsky, and T. Ditmire, *Phys. Rev. Lett.* **84**, 2634 (2000).
4. J. Zweiback, T. E. Cowan, R. A. Smith, J. H. Hartley, R. Howell, C. A. Steinke, G. Hays, K. B. Wharton, J. K. Crane, and T. Ditmire, *Phys. Rev. Lett.* **85**, 3640 (2000).
5. G. Grillon, Ph. Balcou, J.-P. Chambaret, D. Hulin, J. Martino, S. Moustazis, L. Notebaert, M. Pittman, Th. Pussieux, A. Rousse, J.-Ph. Rousseau, S. Sebban, O. Sublemontier, and M. Schmidt, *Phys. Rev. Lett.* **89**, 065005-1 (2002).
6. K. W. Madison, P. K. Patel, D. Price, A. Edens, M. Allen, T. E. Cowan, J. Zweiback, and T. Ditmire, *Phys. Plasmas* **11**, 270 (2004).
7. K. W. Madison, P. K. Patel, M. Allen, D. Price, R. Fitzpatrick, and T. Ditmire, *Phys. Rev. A* **70**, 053201 (2004).
8. H. Y. Lu, J. S. Liu, C. Wang, W. T. Wang, Z. L. Zhou, A. H. Deng, C. Q. Xia, Y. Xu, X. M. Lu, Y. H. Jiang, Y. X. Leng, X. Y. Liang, G. Q. Ni, R. X. Li, and Z. Z. Xu, *Phys. Rev. A* **80**, 051201(R) (2009).
9. H. Lu, J. Liu, C. Wang, W. Wang, Z. Zhou, A. Deng, C. Xia, Y. Xu, Y. Leng, G. Ni, R. Li, and Z. Xu, *Phys. Plasmas* **16**, 083107 (2009).
10. I. Last, and J. Jortner, *Phys. Rev. Lett.* **87**, 033401 (2001).
11. I. Last, and J. Jortner, *Phys. Rev. A* **64**, 063201 (2001).
12. P. B. Parks, T. E. Cowan, R. B. Stephens, and E. M. Campbell, *Phys. Rev. A* **63**, 063203 (2001).
13. J. Davis, G. M. Petrov, and A. L. Velikovich, *Phys. Plasmas* **13**, 064501 (2006).
14. H. Li, J. Liu, Ch. Wang, G. Ni, Ch. J. Kim, R. Li, and Zh. Xu, *J. Phys. B* **40**, 3941 (2007).
15. H. Li, J. Liu, G. Ni, R. Li, and Zh. Xu, *Phys. Rev. A* **79**, 043204 (2009).
16. S. Karsch, S. Düsterer, H. Schwoerer, F. Ewald, D. Habs, M. Hegelich, G. Pretzler, A. Puckhov, K. Witte, and R. Sauerbrey, *Phys. Rev. Lett.* **91**, 015001 (2003).
17. S. Ter-Avetisyan, M. Schnürer, D. Hilscher, U. Jahnke, S. Busch, P. V. Nicles, and W. Sandner, *Phys. Plasmas* **12**, 012702 (2005).
18. I. Last, and J. Jortner, *Phys. Rev. Lett.* **97**, 173401 (2006).
19. I. Last, and J. Jortner, *Phys. Plasmas* **14**, 123102 (2007).
20. I. Last, F. Peano, J. Jortner, and L. O. Silva, *Eur. J. Phys. D* **57**, 327 (2010).
21. G. A. Morou, T. Tajima, and S. V. Bulanov, *Rev. Mod. Phys.* **78**, 309 (2006).
22. I. Last, and J. Jortner, *Phys. Rev. A* **60**, 602215 (1999).

23. A. Heidenreich, I. Last, and J. Jortner, in *Analysis and Control of Ultrafast Photoinduced Processes, Vol. 87*, O. Kühn, and L. Wöste, eds. (Springer, Heidelberg, 2007), p. 575.
24. I. Last, and J. Jortner, *Chem. Phys.* **399**, 218 (2012).
25. I. Last, S. Ron, and J. Jortner, *Phys. Rev. A* **83**, 043202 (2011).
26. S. Ron, I. Last, and J. Jortner, *Phys. Plasmas* **19**, 112707 (2012).
27. T. R. Dittrich, B. A. Hammel, C. J. Keane, R. McEachren, R. E. Turner, S. Haan, and L. J. Suter, *Phys. Rev. Lett.* **73**, 2324 (1994).
28. A. M. Cok, R. S. Craxton, and P. W. McKenty, *Phys. Plasmas* **15**, 082705 (2008).
29. NIF Project Status (2011) September, https://lasers.llnl.gov/newsroom/project_status/2011/september.php.
30. P. Yu-dong, H. Tian-Xuan, L. Huang, Z. Xia-Yu, P. Xiao-Shi, Tang-Qi, S. Zi-Feng, C. Jia-Bin, S. Tian-Ming, C. Ming, Y. Rui-Zhen, H. Xiao-An, L. Chao-Guang, Z. Lu, Z. Jia-Hua, J. Long-Fei, C. Bo-Lun, S. Ming, J. Wei, Y. Bo, Y. Ji, L. Ping, L. Hai-Le, J. Shao-En, D. Yong-Kun, *et al.*, *Phys. Plasmas* **19**, 072708 (2012).
31. D. J. Rose, and M. Clark Jr., *Plasmas and Controlled Fusion* (M. I. T. Press, Cambridge, Massachusetts, 1961).
32. J. Davis, G. M. Petrov, Tz. Petrova, L. Willingale, A. Maksimchuk, and K. Krushelnick, *Plasma Phys. Control. Fusion* **52**, 045015 (2010).
33. S. Eliezer, Z. Henis, and J. M. Martinez-Val, *Nuclear Fusion* **37**, 985 (1997).
34. I. Last, and J. Jortner, *Phys. Rev. A* **75**, 042507 (2007).
35. I. Last, and J. Jortner, *Polish J. Chem.* **82**, 661 (2008).
36. H. H. Andersen, and J. F. Ziegler, *Hydrogen Stopping Powers and Ranges in All Elements* (Pergamon Press, NY, 1977).
37. I. Last, and J. Jortner, *Phys. Rev. A* **73**, 063201 (2006).
38. I. Last, and J. Jortner, *J. Chem. Phys.* **120**, 1336 (2004).
39. J. Davis, and G. M. Petrov, *Plasma Phys. Control. Fusion* **50**, 065016 (2008).